

# Dual Inflation and Bounce Cosmologies Interpretation of Pulsar Timing Array Data

Changhong Li,<sup>1,\*</sup> Junrong Lai,<sup>1</sup> Jinjie Xiang,<sup>1</sup> and Chaofan Wu<sup>1</sup>

<sup>1</sup>*Department of Astronomy, Key Laboratory of Astroparticle Physics of Yunnan Province, School of Physics and Astronomy, Yunnan University, No.2 Cuihu North Road, Kunming, China 650091*

(Dated: February 11, 2025)

This work explores the entire parameter space of a dual scenario that combines generalized inflation and bounce cosmologies. In this scenario, the redshift term of curvature perturbation are phenomenologically generalized to accommodate various model-building of inflation and bounce cosmologies. Performing a Bayesian analysis with data from NANOGrav 15-year, PPTA DR3, EPTA DR2, and IPTA DR2, we identify, for the first time, two groups of regions—each comprising dual regions from inflation and bounce—that can simultaneously explain stochastic gravitational wave background (SGWB) signals detected by pulsar timing arrays and produce scale-invariant curvature perturbations compatible with observations of CMB anisotropies. Bayes factor (BF) calculations indicate that this dual scenario is strongly favored by NG15 data with large BFs over other conventional astrophysical and cosmological sources, such as supermassive black hole binaries, cosmic strings, domain walls, first-order phase transitions, and scalar-induced gravitational waves. Our Bayesian analysis also provides initial evidence of a duality between inflation and bounce cosmologies regarding SGWB. These results offer new insights for model-building in the early universe’s inflation or bounce phases and highlight parameter regions that can be probed by current and future CMB observations and gravitational wave detectors.

**Introduction.** Pulsar Timing Array (PTA) experiments, including NANOGrav [1, 2], EPTA [3, 4], PPTA [5, 6], IPTA [7], and CPTA [8], provide a unique probe into the new physics related to nano-Hertz frequency gravitational waves [9]. Various astrophysical and cosmological sources, including supermassive black hole binaries (SMBH binaries)[10–13], inflationary gravitational waves (IGWs)[14–16], cosmic strings (CS) [17–19], domain walls (DWs) [20–22], first-order phase transitions (FOPT) [23–27], and scalar-induced gravitational waves (SIGWs) [28–30], have been proposed to explain the recently detected stochastic gravitational wave background (SGWB) signals [31, 32]. However, Bayesian analysis suggests that no single source is very strongly preferred over the others [33]. To further explore the physical implications of SGWB signals, a variety of other models have been proposed, including audible axion [34, 35], kination-domination [36, 37], preheating [38, 39], and particle production [40, 41]; see [9] for a comprehensive review and [31, 32] for a concise summary of recent developments.

Among these SGWB candidates, inflationary gravitational waves (IGWs) with a blue-tilted tensor spectrum,  $n_T \simeq 1.8 \pm 0.3$  [42], have been considered a compelling source. However, this interpretation poses a severe challenge to the standard inflation model, as constrained by the “consistency” relations  $n_T \simeq 1 - n_s$  and  $n_T = -r/8$  [32, 42]. Here,  $n_T$  and  $n_s$  denote the spectral indices of tensor and scalar (curvature) perturbations, respectively, and  $r$  represents the tensor-to-scalar ratio of perturbation spectra. This conflict specifically implies that the scale-invariant curvature perturbation, compatible with observations of cosmic microwave background (CMB) anisotropies ( $n_s - 1 = -0.04$  [43–45]), cannot be generated along the blue-tilted primordial gravitational wave [32]. Similar challenges are also evident in other existing inflationary models and various bounce universe models [46–53].

Notably, in a dual scenario combining generalized inflation

and bounce cosmologies [54], a phenomenologically generalized redshift term for curvature perturbations allows for the maintenance of scale invariance, with  $(n_s - 1) \simeq 0$ , despite a blue-tilted tensor spectrum of  $n_T = 1.8 \pm 0.3$ . This feature renders the scenario capable of explaining the SGWB signal detected in PTAs and being compatible with observations of CMB anisotropies simultaneously. More specifically, as an extension of Wands’s duality [55–58], this scenario extends the standard Hubble horizon,  $\mathcal{H}^{-1} \equiv (aH)^{-1}$ , to an “effective” Hubble horizon,  $\mathcal{H}_u^{-1} \equiv |aH|^{-1}$ , to incorporate the collapsing phase of bounce cosmologies ( $aH < 0$ ). Furthermore, to accommodate various model-building approaches in inflation and bounce cosmologies, the red-shift term coefficient of curvature perturbation modes  $\chi_k$  is phenomenologically generalized from  $3H$  to  $mH$ , leading to [54]:

$$\ddot{\chi}_k + mH\dot{\chi}_k + \frac{k^2}{a^2}\chi_k = 0, \quad a(\eta) \propto \eta^\nu. \quad (1)$$

Here,  $k$  represents the wave-vector of curvature perturbation modes  $\chi_k$ , while  $H$  denotes the Hubble parameter. The parameter  $\nu$  signifies the power-law index of the scale factor  $a(\eta)$  in terms of conformal time  $\eta$ , characterizing the perturbation horizon-exiting phase of various cosmic evolutions. The parameter  $m$  serves as the damping parameter, which varies with the specific generalization of inflation and bounce cosmology models, characterizing various levels of damping behavior, from enhanced to suppressed effects. For instance, in the standard inflation scenario,  $m = 3$ , whereas in the coupled scalar-tachyon bounce (CSTB) model,  $m = 0$  [54, 59, 60]. This phenomenological generalization of the red-shifted term unifies various generalized inflation and bounce models into a single parameter space  $(m, \nu)$ , as illustrated in Fig.4. It provides an opportunity to examine the entire parameter space to find models capable of explaining both the SGWB signal and CMB anisotropies simultaneously, addressing challenges faced by existing single inflation or bounce cosmological models.

In this work, we explore the novel possibility that stochastic gravitational wave background (SGWB) signals originate from a dual scenario of generalized inflation and bounce cosmologies. We thoroughly investigate the entire parameter space of this dual scenario, aiming to elucidate its potential in explaining both SGWB signals and CMB anisotropies simultaneously. Our methodology involves imposing the scale-invariance condition for the curvature perturbation spectrum and conducting Bayesian analyses using data from NANOGrav 15-year, PPTA DR3, EPTA DR2, and IPTA DR2 [61–68].

For the first time, we identify two groups of four regions within this dual scenario that can explain SGWB signals and CMB anisotropies simultaneously. Initially, within the conventional parameter space  $(n_T, r)$ , we perform Bayesian analysis with PTA data to identify the region for the dual scenario, depicted in Fig.2 (a), consistent with previous studies. Subsequently, within the parameter space  $(w, r)$ , Bayesian analysis with PTA data isolates inflationary and bounce regions capable of explaining SGWB signals, shown in Fig.2 (b). Ultimately, by enforcing scale invariance conditions for the curvature perturbation spectrum and conducting further Bayesian analyses with PTA data, we delineate two groups of four regions that can concurrently account for SGWB signals and CMB anisotropies across the  $(m, \nu)$  parameter space, as depicted in Fig. 2 (c). These two groups encompass stable and dynamic scale-invariant solutions, with each group comprising dual regions from inflation and bounce cosmologies.

In Fig. 1, we showcase two examples from the  $1\sigma$  posterior distribution region of our findings within the parameter spaces  $(w, r)$  (refer to Fig. 2(b)) and four examples from  $(m, r)$  (refer to Fig. 2(c)), demonstrating their potential to elucidate the SGWB signals detected by PTAs. As previously mentioned, the latter four examples can simultaneously address both SGWB signals and CMB anisotropies.

To assess the credibility of this novel scenario against other astrophysical and cosmological sources, we compute the Bayes factors (BFs) between them. Our analysis reveals robust support for this dual scenario from the NANOGrav 15-year data, with significantly higher BFs compared to alternative sources such as supermassive black hole binaries, cosmic strings, domain walls, first-order phase transitions, and scalar-induced gravitational waves, as listed in Tab. I. Moreover, BFs computed within the dual scenario regions, all close to unity, suggest initial evidence of a duality between inflation and bounce cosmologies in explaining SGWB, as listed in Tab. II. These findings underscore the importance of further investigation into this dual scenario and its implications for future model-building in the early universe’s inflation or bounce phases. Additionally, we highlight parameter regions ripe for exploration by current and future CMB observations and gravitational wave detectors, noting some regions already excluded by recent observations.

**Dual Scenario Interpretation of SGWB Spectrum** The SGWB spectrum induced by the primordial gravitational wave from

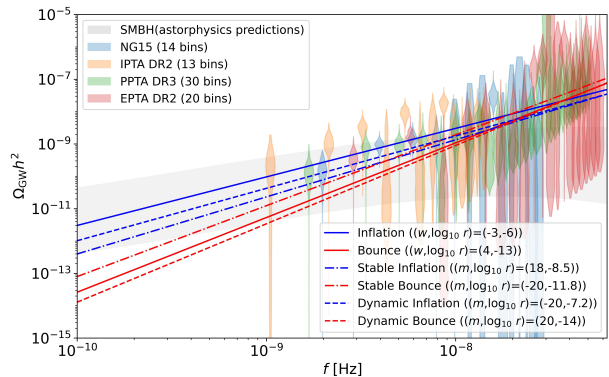


FIG. 1. Examples from the  $1\sigma$  posterior distribution region of our findings within the parameter spaces  $(w, r)$  and  $(m, r)$  (see Fig.2 (b) and (c)), illustrating their potential to elucidate the SGWB signals detected by PTAs. The “violin” diagrams depict the posterior probability distribution of the SGWB energy density across various frequency bins in these PTAs’ datasets [61–68], with shaded regions representing astrophysical predictions from supermassive black hole (SMBH) binaries [69].

inflation and bounce cosmologies is given by [9]:

$$\Omega_{\text{GW}}(f)h^2 = \frac{3}{128} \Omega_{\gamma 0} h^2 \cdot r \cdot \mathcal{P}_{\mathcal{R}} \left( \frac{f}{f_*} \right)^{n_T} \left[ \frac{1}{2} \left( \frac{f_{\text{eq}}}{f} \right)^2 + \frac{16}{9} \right], \quad (2)$$

where  $r$  and  $n_T$  are, respectively, the tensor-to-scalar ratio ( $r \equiv \mathcal{P}_h/\mathcal{P}_{\mathcal{R}}$ ) and the spectral index of the primordial tensor spectrum ( $\mathcal{P}_h \propto (k/k_*)^{n_T}$ ) for these inflation and bounce cosmologies, measured at the pivot scale  $k_* = 0.05 \text{Mpc}^{-1}$ .  $\mathcal{P}_{\mathcal{R}} = 2 \times 10^{-9}$  is the amplitude of the curvature perturbation spectrum at  $k = k_*$  [9].  $f_* = 1.55 \times 10^{-15} \text{Hz}$  is the frequency today corresponding to  $k_*$ , and  $f_{\text{eq}} = 2.01 \times 10^{-17} \text{Hz}$  represents the frequency today corresponding to matter-radiation equality.  $\Omega_{\gamma 0} = 2.474 \times 10^{-5} h^{-2}$  is the energy density fraction of radiation today, and  $h = 0.677$  is the reduced Hubble constant.

Initially, we performed a Bayesian analysis to fit Eq.(2) with data from the NANOGrav 15-year, EPTA DR2, PPTA DR3, and IPTA DR2 pulsar timing arrays (PTAs hereafter), reproducing the 2D joint posterior probability distribution within the conventional parameter space  $(n_T, r)$  in Fig. 2 (a). This distribution is consistent with previous studies (e.g., Fig. 2 in Ref. [42]). Notably, this dual scenario interprets the viable range of  $n_T$  not only from inflation ( $n_T = \frac{4}{3w+1} + 2 < 2$  for the accelerating expansion phase with  $w < -\frac{1}{3}$ ) but also from bounce ( $n_T = \frac{4}{3w+1} + 2 > 2$  for the collapsing contraction phase with  $w > -\frac{1}{3}$ ) cosmologies, see Eq.(3). The details of all Bayesian analysis in this work can be found in the Supplemental Material.

Subsequently, in this work, to resolve the degeneracy between inflation and bounce cosmologies within the parameter space, we express the tensor spectral index  $n_T$  in terms of the

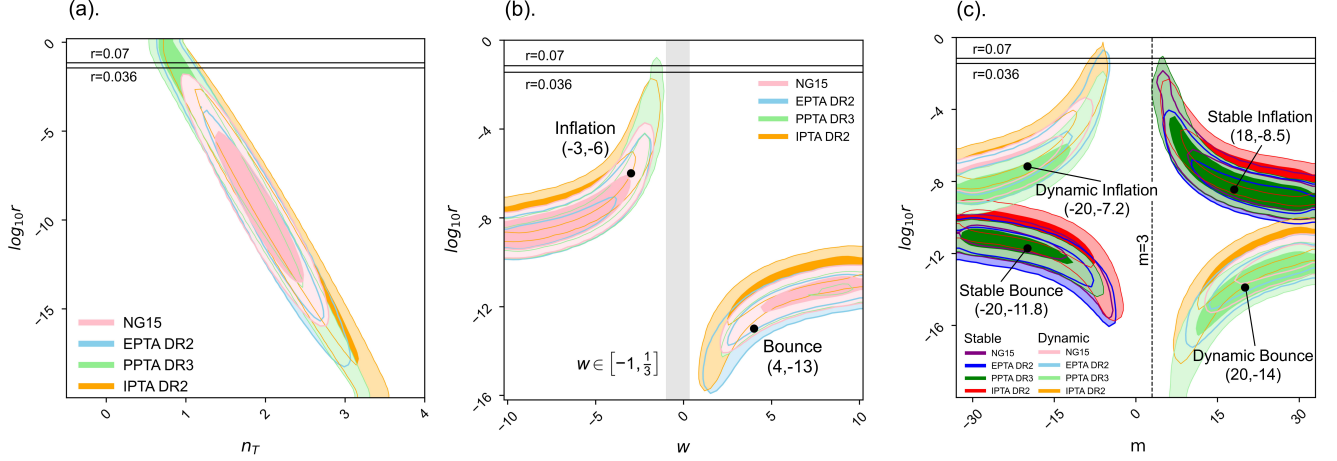


FIG. 2. Posterior distributions (at 68% and 95% confidence levels) in the parameter spaces  $(n_T, r)$ ,  $(w, r)$ , and  $(m, r)$  for the dual scenario of generalized inflation and bounce cosmologies. Bayesian analyses across PTA datasets employed three different approaches: direct fitting of Eq.(2), fitting Eq.(2) with Eq.(3), and fitting Eq.(2) with Eq.(5) and Eq.(6). Sub-figure (a) depicts the viable region of this dual scenario within the conventional parameter space  $(n_T, r)$  explaining the SGWB signal. Sub-figure (b) delineates isolated regions for inflation and bounce cosmologies within  $(w, r)$  parameter space capable of explaining the SGWB signal. Sub-figure (c) reveals two groups of four regions in  $(m, r)$  parameter space, newly identified in this dual scenario, capable of explaining SGWB signals and generating a scale-invariant curvature perturbation spectrum concurrently. These sub-figures demonstrate the gradual resolution of degeneracy resulting from inflation-bounce damping-temporal duality in parameter space.

equation of state  $w$ , as follows:

$$n_T = \frac{4}{3w+1} + 2. \quad (3)$$

This formulation mirrors the conventional relation derived in inflationary cosmologies ( $\dot{a} > 0$  and  $\ddot{a} > 0$ ;  $w < -\frac{1}{3}$ ), as discussed in Refs. [14] and [42]. Notably, this dual scenario also incorporates the contraction phase of bounce cosmologies ( $\dot{a} < 0$  and  $\ddot{a} < 0$ ;  $w > -\frac{1}{3}$ ), extending the applicability of the model.

Substituting Eq.(3) into Eq.(2) and performing a Bayesian analysis with data from PTAs, we identified two isolated regions that can explain the SGWB signals within the parameter space  $(w, r)$ , as illustrated in Fig.2(b): the inflation (top left,  $w < -\frac{1}{3}$ ) featuring larger  $r$  values and bounce cosmologies (bottom left,  $w > -\frac{1}{3}$ ) exhibiting smaller  $r$  values, respectively. Notably, the conventional parameter region of the equation of state (EoS) encompassing traditional cosmological inflation and bounce models,  $-1 < w < \frac{1}{3}$ , is not favored by this model-independent Bayesian analysis, as illustrated by the shaded gray region in Fig.2(b). This observation suggests that standard inflation and matter bounce models [48, 49] are unable to account for the SGWB signal, corroborating findings from previous studies [32]. However, across a wider parameter space of  $w$ , our results provide the first systematic demonstration of the potential to account for SGWB signals within inflationary and bounce cosmologies. Additionally, further regions of the inflationary parameter space of  $r$ , beyond those currently excluded by observations of CMB anisotropies at  $r = 0.07$  based on WMAP and Planck data,

and at  $r = 0.036$  based on BICEP+ ( $-1.92 < w < -1.18$  for  $2\sigma$  C.L. range of PPTA DR3 dataset), will be explored by upcoming experiments such as CMB-S4.

Ultimately, by enforcing scale invariance conditions for the curvature perturbation spectrum and conducting further Bayesian analyses with PTA data, we identify the viable regions within the dual scenario that can concurrently account for SGWB signals and CMB anisotropies. Specifically, in this dual scenario, the spectral index of the curvature perturbation spectrum,  $\mathcal{P}_{\mathcal{R}} \propto k^{n_s-1}$ , is given by (cf. Eq.(4.2) and Eq.(4.3) in Ref. [54], also see Supplemental Material),

$$n_s - 1 = -|(m-1)\nu - 1| + 3, \quad (4)$$

where  $\nu$  is the power-law index of the scale factor and  $m$  is the damping parameter of the generalized redshift term. Applying the scale-invariance condition,  $n_s - 1 = 0$  (see Supplemental Material for the  $n_s - 1 = -0.04$  case), one can derive two solutions from Eq.(4) (cf. Eq.(4.5) and Eq.(4.6) in Ref. [54]): one is a time-independent (stable) scale-invariant solution ( $\mathcal{P}_{\mathcal{R}} \propto k^0 \eta^0$ ),

$$m = -\frac{2}{\nu} + 1, \quad (5)$$

and the other is a time-dependent (dynamic) scale-invariant solution ( $\mathcal{P}_{\mathcal{R}} \propto k^0 \eta^{-2(m-1)\nu+2}$ ),

$$m = \frac{4}{\nu} + 1. \quad (6)$$

In these two solutions, the damping parameter  $m$ , which characterizes the enhanced or suppressed damping effect, balances

the power index of the scale factor  $\nu$ , which characterizes the temporal effect from the cosmic background, to generate scale-invariant curvature perturbation spectra compatible with CMB anisotropy observations. For instance, the standard inflation model  $(m, \nu) = (3, -1)$  and the CSTB model  $(m, \nu) = (0, 2)$  correspond to the stable solution in Eq.(5), while the matter bounce model  $(m, \nu) = (3, 2)$  with  $\mathcal{P}_{\mathcal{R}} \propto k^0 \eta^{-6}$  corresponds to the dynamic solution in Eq.(6) [48, 49].

Utilizing the relation  $n_T = 2\nu + 2$ , we substituted Eq.(5) and Eq.(6) into Eq.(2) and performed further Bayesian analysis with data from PTAs. For the first time, we identified two groups of four regions—each group comprising dual regions from inflation and bounce—that can simultaneously explain the SGWB signal and CMB anisotropies, as illustrated in Fig.2(c). The stable and dynamic scale-invariant groups, which can also explain the SGWB signal, are depicted as the darker (Eq.(5)) and lighter (Eq. (6)) colored regions, respectively. This finding addresses the challenge faced by existing single inflation and bounce cosmological models.

Furthermore, we observe that around the standard damping parameter value,  $m = 3$ , the parameter space has been excluded by data from PTAs, corroborating numerous previous studies. For general values of  $m$ , certain parameter regions associated with  $r$  have been ruled out by current observations of CMB anisotropies (as constrained by  $r = 0.036$  from BICEP+,  $m$  has been excluded for  $[-8.4, -4.7]$  and  $[4.1, 5.7]$  for the  $2\sigma$  confidence level range of the PPTA DR3 dataset). However, significant unexplored territories remain, which upcoming experiments like CMB-S4 are well-positioned to investigate. The overlap of colored regions between inflation and bounce arises from uncertainties in each PTA’s dataset. For each dataset, they are not overlapping.

**Model Comparison** In Table I, we present the Bayes factors (BF)  $B_{\alpha_j} = \text{evidence}[H_\alpha]/\text{evidence}[H_j]$ , obtained from a Bayesian model selection and comparison analysis using NG15 data. Here,  $H_\alpha$  denotes each case within scenario  $\alpha$  (including the Dual Scenario in  $(w, r)$  prior, Stable, Dynamic, and Dual Scenario in  $(m, r)$  prior), and  $H_j$  refers to each model  $j$  (including SMBHBs, CS, DW, FOPT, and SIGW). The results indicate that all Bayes factors (BFs) are larger than 30, suggesting that the dual scenario fits the NG15 data much better than other compelling astrophysical and cosmological sources of SGWB. This warrants further investigation into the potential of this dual scenario as a source and underscores its implications for future model-building in the early universe’s inflation or bounce phases. In the Supplemental Material, we provide BF matrices for all model comparisons across NG15, EPTA DR2, PPTA DR3, and IPTA DR2 with their prior ranges. They are not so optimistic like NG15 but still provide a substantial support for the dual scenario.

Additionally, in Table II, we present the Bayes factors comparing inflation to bounce, stable scale-invariant inflation to bounce, dynamic scale-invariant inflation to bounce, and stable to dynamic scale-invariant solutions, respectively. (R/L) represents the region on the right-hand side relative to the region on the left-hand side. The results, all close to 1, pro-

vide initial evidence of strong dualities between inflation and bounce models concerning SGWB, a duality previously established only for curvature perturbations [54–58]. This finding would strength the motivation for current and future model-building of bounce cosmologies.

**Conclusion** This work explored the entire parameter space of a dual scenario combining generalized inflation and bounce cosmologies. By performing Bayesian analysis utilizing data from NANOGrav 15-year, PPTA DR3, EPTA DR2, and IPTA DR2, we have, for the first time, identified two groups of four distinct regions—each group comprising dual regions from both inflation and bounce—that can simultaneously explain SGWB signals detected by PTAs and CMB anisotropies measured by WMAP and Planck satellites. This approach addresses the challenges faced by existing conventional inflation or bounce models.

The Bayes factor (BF) calculations indicate that this dual scenario is strongly favored by NG15 data, with large BFs compared to other traditional astrophysical and cosmological sources such as SMBH binaries, CS, DW, FOPT, and SIGW. This finding warrants further investigation of this dual scenario as a compelling source and offers new insights for future model-building of inflation and bounce cosmological models. Additionally, the BFs between each region of the dual scenario, all close to unity, suggest strong dualities between inflation and bounce regarding SGWB, previously established only for curvature perturbations. This strengthens the motivation for bounce cosmology.

In addition to this initial exploration of the dual scenario merging inflation and bounce cosmologies, further investigations are imperative. These should focus on the impact of the reheating process and the bounce point, as well as the constraints imposed by  $\Delta N_{\text{eff}}$  and the necessity of a broken power law of SGWB spectra [70] to accommodate LIGO/Virgo/KAGRA (LVK) observations of the stochastic gravitational wave background (SGWB). Such studies are essential for establishing robust conclusions. Notably, although in some parameter spaces, the value of  $r$  predicted by this scenario, especially for bounce cosmology, is too small to be detected ( $r < 10^{-10}$ ), the predicted SGWB signals and the broken scale of the power law can still be explored at higher frequencies by LISA, aLIGO, and similar observatories.

We would like to thank Yann Gouttenoire and Junchao Zong for their valuable communications on the data analysis, and Jing Shu for his many encouragements. C.L. is supported by the NSFC under Grants No.11963005 and No. 11603018, by Yunnan Provincial Foundation under Grants No.202401AT070459, No.2019FY003005, and No.2016FD006, by Young and Middle-aged Academic and Technical Leaders in Yunnan Province Program, by Yunnan Provincial High level Talent Training Support Plan Youth Top Program, by Yunnan University Donglu Talent Young Scholar, and by the NSFC under Grant No.11847301 and by the Fundamental Research Funds for the Central Universities under Grant No. 2019CDJDWL0005.

TABLE I. Bayes factors (BF) comparing our model with others using NG15 data

Bayes factor	SMBHBs	CS	DW	FOPT	SIGW
<b>Dual Scenario</b> ( $w, r$ )	$94.6 \pm 34.9$	$461.6 \pm 127.2$	$318.8 \pm 73.2$	$61.4 \pm 11.6$	$65.2 \pm 12.4$
<b>Stable Solutions</b>	$81.5 \pm 32.3$	$397.7 \pm 117.8$	$274.7 \pm 67.8$	$52.9 \pm 10.7$	$56.2 \pm 10.7$
<b>Dynamic Solutions</b>	$49.4 \pm 17.3$	$240.7 \pm 63.2$	$166.3 \pm 36.4$	$32.0 \pm 6.8$	$34.0 \pm 6.5$
<b>Dual Scenario</b> ( $m, r$ )	$83.9 \pm 30.9$	$409.0 \pm 112.7$	$282.6 \pm 64.9$	$54.4 \pm 10.3$	$57.8 \pm 11.0$

TABLE II. Bayes Factors Comparing Each Regions of Dual Scenario Across Different PTA Datasets

Bayes factor	NG15	EPTA	PPTA	IPTA
<b>Bounce/Inflation</b>	$0.95 \pm 0.22$	$1.23 \pm 0.32$	$1.48 \pm 0.61$	$1.37 \pm 0.36$
<b>Stable(R/L)</b>	$0.94 \pm 0.24$	$0.89 \pm 0.22$	$0.95 \pm 0.43$	$1.01 \pm 0.42$
<b>Dynamic(R/L)</b>	$0.63 \pm 0.16$	$1.41 \pm 0.27$	$1.24 \pm 0.39$	$1.08 \pm 0.41$
<b>Stable/Dynamic</b>	$1.65 \pm 0.46$	$1.33 \pm 0.44$	$1.23 \pm 0.56$	$1.49 \pm 0.79$

\* changhongli@ynu.edu.cn

- [1] N. S. Pol *et al.* [NANOGrav], “Astrophysics Milestones for Pulsar Timing Array Gravitational-wave Detection,” *Astrophys. J. Lett.* **911**, no.2, L34 (2021) [arXiv:2010.11950 [astro-ph.HE]].
- [2] G. Agazie *et al.* [NANOGrav], “The NANOGrav 15 yr Data Set: Evidence for a Gravitational-wave Background,” *Astrophys. J. Lett.* **951**, no.1, L8 (2023) [arXiv:2306.16213 [astro-ph.HE]].
- [3] S. Chen *et al.* [EPTA], “Common-red-signal analysis with 24-yr high-precision timing of the European Pulsar Timing Array: inferences in the stochastic gravitational-wave background search,” *Mon. Not. Roy. Astron. Soc.* **508**, no.4, 4970-4993 (2021) doi:10.1093/mnras/stab2833 [arXiv:2110.13184 [astro-ph.HE]].
- [4] J. Antoniadis *et al.* [EPTA and InPTA:], “The second data release from the European Pulsar Timing Array - III. Search for gravitational wave signals,” *Astron. Astrophys.* **678**, A50 (2023) [arXiv:2306.16214 [astro-ph.HE]].
- [5] B. Goncharov, R. M. Shannon, D. J. Reardon, G. Hobbs, A. Zic, M. Bailes, M. Curylo, S. Dai, M. Kerr and M. E. Lower, *et al.* “On the Evidence for a Common-spectrum Process in the Search for the Nanohertz Gravitational-wave Background with the Parkes Pulsar Timing Array,” *Astrophys. J. Lett.* **917**, no.2, L19 (2021) [arXiv:2107.12112 [astro-ph.HE]].
- [6] D. J. Reardon, A. Zic, R. M. Shannon, G. B. Hobbs, M. Bailes, V. Di Marco, A. Kapur, A. F. Rogers, E. Thrane and J. Askew, *et al.* *Astrophys. J. Lett.* **951**, no.1, L6 (2023) doi:10.3847/2041-8213/acdd02 [arXiv:2306.16215 [astro-ph.HE]].
- [7] J. Antoniadis, Z. Arzoumanian, S. Babak, M. Bailes, A. S. B. Nielsen, P. T. Baker, C. G. Bassa, B. Becsy, A. Berthereau and M. Bonetti, *et al.* “The International Pulsar Timing Array second data release: Search for an isotropic gravitational wave background,” *Mon. Not. Roy. Astron. Soc.* **510**, no.4, 4873-4887 (2022) [arXiv:2201.03980 [astro-ph.HE]].
- [8] H. Xu, S. Chen, Y. Guo, J. Jiang, B. Wang, J. Xu, Z. Xue, R. N. Caballero, J. Yuan and Y. Xu, *et al.* “Searching for the Nano-Hertz Stochastic Gravitational Wave Background with the Chinese Pulsar Timing Array Data Release I,” *Res. Astron. Astrophys.* **23**, no.7, 075024 (2023) [arXiv:2306.16216 [astro-ph.HE]].
- [9] C. Caprini and D. G. Figueroa, “Cosmological Backgrounds of Gravitational Waves,” *Class. Quant. Grav.* **35**, no.16, 163001 (2018) [arXiv:1801.04268 [astro-ph.CO]].
- [10] A. Sesana, “Insights into the astrophysics of supermassive black hole binaries from pulsar timing observations,” *Class. Quant. Grav.* **30**, 224014 (2013) doi:10.1088/0264-9381/30/22/224014 [arXiv:1307.2600 [astro-ph.CO]].
- [11] L. Z. Kelley, L. Blecha, L. Hernquist, A. Sesana and S. R. Taylor, “The Gravitational Wave Background from Massive Black Hole Binaries in Illustris: spectral features and time to detection with pulsar timing arrays,” *Mon. Not. Roy. Astron. Soc.* **471**, no.4, 4508-4526 (2017) doi:10.1093/mnras/stx1638 [arXiv:1702.02180 [astro-ph.HE]].
- [12] S. Chen, A. Sesana and C. J. Conselice, “Constraining astrophysical observables of Galaxy and Supermassive Black Hole Binary Mergers using Pulsar Timing Arrays,” *Mon. Not. Roy. Astron. Soc.* **488**, no.1, 401-418 (2019) [arXiv:1810.04184 [astro-ph.GA]].
- [13] S. Burke-Spolaor, S. R. Taylor, M. Charisi, T. Dolch, J. S. Hazboun, A. M. Holgado, L. Z. Kelley, T. J. W. Lazio, D. R. Madison and N. Mc Mann, *et al.* *Astron. Astrophys. Rev.* **27**, no.1, 5 (2019) [arXiv:1811.08826 [astro-ph.HE]].
- [14] W. Zhao, Y. Zhang, X. P. You and Z. H. Zhu, “Constraints of relic gravitational waves by pulsar timing arrays: Forecasts for the FAST and SKA projects,” *Phys. Rev. D* **87**, no.12, 124012 (2013) [arXiv:1303.6718 [astro-ph.CO]].
- [15] M. C. Guzzetti, N. Bartolo, M. Liguori and S. Matarrese, “Gravitational waves from inflation,” *Riv. Nuovo Cim.* **39**, no.9, 399-495 (2016) [arXiv:1605.01615 [astro-ph.CO]].
- [16] S. Vagnozzi, “Implications of the NANOGrav results for inflation,” *Mon. Not. Roy. Astron. Soc.* **502**, no.1, L11-L15 (2021) doi:10.1093/mnras/slaa203 [arXiv:2009.13432 [astro-ph.CO]].
- [17] X. Siemens, V. Mandic and J. Creighton, “Gravitational wave stochastic background from cosmic (super)strings,” *Phys. Rev. Lett.* **98**, 111101 (2007) doi:10.1103/PhysRevLett.98.111101 [arXiv:astro-ph/0610920 [astro-ph]].
- [18] Y. Cui, M. Lewicki, D. E. Morrissey and J. D. Wells, “Probing the pre-BBN universe with gravitational waves from cosmic strings,” *JHEP* **01**, 081 (2019) [arXiv:1808.08968 [hep-ph]].
- [19] Y. Gouttenoire, G. Servant and P. Simakachorn, “Beyond the Standard Models with Cosmic Strings,” *JCAP* **07**, 032 (2020) [arXiv:1912.02569 [hep-ph]].
- [20] T. Hiramatsu, M. Kawasaki and K. Saikawa, “On the estimation of gravitational wave spectrum from cosmic domain walls,” *JCAP* **02**, 031 (2014) [arXiv:1309.5001 [astro-ph.CO]].
- [21] R. Z. Ferreira, A. Notari, O. Pujolas and F. Rompineve, “Gravitational waves from domain walls in Pulsar Timing Array datasets,” *JCAP* **02**, 001 (2023) doi:10.1088/1475-

- 7516/2023/02/001 [arXiv:2204.04228 [astro-ph.CO]].
- [22] L. Bian, S. Ge, C. Li, J. Shu and J. Zong, “Domain Wall Network: A Dual Solution for Gravitational Waves and Hubble Tension?,” [arXiv:2212.07871 [hep-ph]].
- [23] M. Hindmarsh, S. J. Huber, K. Rummukainen and D. J. Weir, “Gravitational waves from the sound of a first order phase transition,” *Phys. Rev. Lett.* **112**, 041301 (2014) [arXiv:1304.2433 [hep-ph]].
- [24] M. Hindmarsh, S. J. Huber, K. Rummukainen and D. J. Weir, *Phys. Rev. D* **92**, no.12, 123009 (2015) doi:10.1103/PhysRevD.92.123009 [arXiv:1504.03291 [astro-ph.CO]].
- [25] M. Hindmarsh, S. J. Huber, K. Rummukainen and D. J. Weir, *Phys. Rev. D* **96**, no.10, 103520 (2017) [erratum: *Phys. Rev. D* **101**, no.8, 089902 (2020)] [arXiv:1704.05871 [astro-ph.CO]].
- [26] C. Caprini, M. Hindmarsh, S. Huber, T. Konstandin, J. Koza-czuk, G. Nardini, J. M. No, A. Petiteau, P. Schwaller and G. Servant, *et al.* “Science with the space-based interferometer eLISA. II: Gravitational waves from cosmological phase transitions,” *JCAP* **04**, 001 (2016) [arXiv:1512.06239 [astro-ph.CO]].
- [27] Y. Gouttenoire, “First-Order Phase Transition Interpretation of Pulsar Timing Array Signal Is Consistent with Solar-Mass Black Holes,” *Phys. Rev. Lett.* **131**, no.17, 17 (2023) [arXiv:2307.04239 [hep-ph]].
- [28] K. N. Ananda, C. Clarkson and D. Wands, “The Cosmological gravitational wave background from primordial density perturbations,” *Phys. Rev. D* **75**, 123518 (2007) [arXiv:gr-qc/0612013 [gr-qc]].
- [29] D. Baumann, P. J. Steinhardt, K. Takahashi and K. Ichiki, “Gravitational Wave Spectrum Induced by Primordial Scalar Perturbations,” *Phys. Rev. D* **76**, 084019 (2007) [arXiv:hep-th/0703290 [hep-th]].
- [30] K. Kohri and T. Terada, “Semianalytic calculation of gravitational wave spectrum nonlinearly induced from primordial curvature perturbations,” *Phys. Rev. D* **97**, no.12, 123532 (2018) [arXiv:1804.08577 [gr-qc]].
- [31] A. Afzal *et al.* [NANOGrav], “The NANOGrav 15 yr Data Set: Search for Signals from New Physics,” *Astrophys. J. Lett.* **951**, no.1, L11 (2023) [arXiv:2306.16219 [astro-ph.HE]].
- [32] D. G. Figueroa, M. Pieroni, A. Ricciardone and P. Simakachorn, “Cosmological Background Interpretation of Pulsar Timing Array Data,” *Phys. Rev. Lett.* **132**, no.17, 171002 (2024) [arXiv:2307.02399 [astro-ph.CO]].
- [33] L. Bian, S. Ge, J. Shu, B. Wang, X. Y. Yang and J. Zong, “Gravitational wave sources for pulsar timing arrays,” *Phys. Rev. D* **109**, no.10, L101301 (2024) [arXiv:2307.02376 [astro-ph.HE]].
- [34] C. S. Machado, W. Ratzinger, P. Schwaller and B. A. Stefanek, “Audible Axions,” *JHEP* **01**, 053 (2019) [arXiv:1811.01950 [hep-ph]].
- [35] C. S. Machado, W. Ratzinger, P. Schwaller and B. A. Stefanek, “Gravitational wave probes of axionlike particles,” *Phys. Rev. D* **102**, no.7, 075033 (2020) [arXiv:1912.01007 [hep-ph]].
- [36] R. T. Co, D. Dunsky, N. Fernandez, A. Ghalsasi, L. J. Hall, K. Harigaya and J. Shelton, *JHEP* **09**, 116 (2022) [arXiv:2108.09299 [hep-ph]].
- [37] V. K. Oikonomou, “Flat energy spectrum of primordial gravitational waves versus peaks and the NANOGrav 2023 observation,” *Phys. Rev. D* **108**, no.4, 043516 (2023) [arXiv:2306.17351 [astro-ph.CO]].
- [38] L. Bethke, D. G. Figueroa and A. Rajantie, “Anisotropies in the Gravitational Wave Background from Preheating,” *Phys. Rev. Lett.* **111**, no.1, 011301 (2013) [arXiv:1304.2657 [astro-ph.CO]].
- [39] P. Adshead, J. T. Giblin, M. Pieroni and Z. J. Weiner, *Phys. Rev. Lett.* **124**, no.17, 171301 (2020) doi:10.1103/PhysRevLett.124.171301 [arXiv:1909.12843 [astro-ph.CO]].
- [40] E. Dimastrogiovanni, M. Fasiello and T. Fujita, “Primordial Gravitational Waves from Axion-Gauge Fields Dynamics,” *JCAP* **01**, 019 (2017) [arXiv:1608.04216 [astro-ph.CO]].
- [41] G. D’Amico, N. Kaloper and A. Westphal, “General double monodromy inflation,” *Phys. Rev. D* **105**, no.10, 103527 (2022) [arXiv:2112.13861 [hep-th]].
- [42] S. Vagnozzi, “Inflationary interpretation of the stochastic gravitational wave background signal detected by pulsar timing array experiments,” *JHEAp* **39**, 81-98 (2023) [arXiv:2306.16912 [astro-ph.CO]].
- [43] E. Komatsu *et al.* [WMAP], “Seven-Year Wilkinson Microwave Anisotropy Probe (WMAP) Observations: Cosmological Interpretation,” *Astrophys. J. Suppl.* **192**, 18 (2011)
- [44] P. A. R. Ade *et al.* [Planck], “Planck 2015 results. XIII. Cosmological parameters,” *Astron. Astrophys.* **594**, A13 (2016)
- [45] N. Aghanim *et al.* [Planck], “Planck 2018 results. VI. Cosmological parameters,” *Astron. Astrophys.* **641**, A6 (2020) [erratum: *Astron. Astrophys.* **652**, C4 (2021)] [arXiv:1807.06209 [astro-ph.CO]].
- [46] R. H. Brandenberger, A. Nayeri, S. P. Patil and C. Vafa, “Tensor Modes from a Primordial Hagedorn Phase of String Cosmology,” *Phys. Rev. Lett.* **98**, 231302 (2007) [arXiv:hep-th/0604126 [hep-th]].
- [47] R. H. Brandenberger, A. Nayeri and S. P. Patil, “Closed String Thermodynamics and a Blue Tensor Spectrum,” *Phys. Rev. D* **90**, no.6, 067301 (2014) [arXiv:1403.4927 [astro-ph.CO]].
- [48] R. Brandenberger, “Matter Bounce in Horava-Lifshitz Cosmology,” *Phys. Rev. D* **80**, 043516 (2009) [arXiv:0904.2835 [hep-th]].
- [49] Y. F. Cai, R. Brandenberger and X. Zhang, “The Matter Bounce Curvaton Scenario,” *JCAP* **03**, 003 (2011) [arXiv:1101.0822 [hep-th]].
- [50] J. Khoury, B. A. Ovrut, P. J. Steinhardt and N. Turok, “The Ekpyrotic universe: Colliding branes and the origin of the hot big bang,” *Phys. Rev. D* **64**, 123522 (2001) [arXiv:hep-th/0103239 [hep-th]].
- [51] Y. T. Wang, Y. Cai, Z. G. Liu and Y. S. Piao, “Probing the primordial universe with gravitational waves detectors,” *JCAP* **01**, 010 (2017) [arXiv:1612.05088 [astro-ph.CO]].
- [52] G. Calcagni and S. Kuroyanagi, “Stochastic gravitational-wave background in quantum gravity,” *JCAP* **03**, 019 (2021) [arXiv:2012.00170 [gr-qc]].
- [53] G. Cabass, L. Pagano, L. Salvati, M. Gerbino, E. Giusarma and A. Melchiorri, “Updated Constraints and Forecasts on Primordial Tensor Modes,” *Phys. Rev. D* **93**, no.6, 063508 (2016) [arXiv:1511.05146 [astro-ph.CO]].
- [54] C. Li and Y. K. E. Cheung, “The scale invariant power spectrum of the primordial curvature perturbations from the coupled scalar tachyon bounce cosmos,” *JCAP* **07**, 008 (2014) [arXiv:1401.0094 [gr-qc]].
- [55] D. Wands, “Duality invariance of cosmological perturbation spectra,” *Phys. Rev. D* **60**, 023507 (1999) [arXiv:gr-qc/9809062 [gr-qc]].
- [56] F. Finelli and R. Brandenberger, “On the generation of a scale invariant spectrum of adiabatic fluctuations in cosmological models with a contracting phase,” *Phys. Rev. D* **65**, 103522 (2002) [arXiv:hep-th/0112249 [hep-th]].
- [57] L. A. Boyle, P. J. Steinhardt and N. Turok, “A New duality relating density perturbations in expanding and contract-



- ing Friedmann cosmologies,” *Phys. Rev. D* **70**, 023504 (2004) [arXiv:hep-th/0403026 [hep-th]].
- [58] R. N. Raveendran, “Conserved cosmological perturbations in ultraslow-roll inflation and bouncing scenarios,” *Phys. Rev. D* **109**, no.4, 043505 (2024) [arXiv:2312.01425 [astro-ph.CO]].
- [59] C. Li, L. Wang and Y. K. E. Cheung, “Bound to bounce: A coupled scalar–tachyon model for a smooth bouncing/cyclic universe,” *Phys. Dark Univ.* **3**, 18-33 (2014) [arXiv:1101.0202 [gr-qc]].
- [60] N. Zhang and Y. K. E. Cheung, “Primordial Gravitational Waves Spectrum in the Coupled-Scalar-Tachyon Bounce Universe,” *Eur. Phys. J. C* **80**, no.2, 100 (2020) [arXiv:1901.06423 [gr-qc]].
- [61] Stephen R. Taylor, Sarah J. Vigelan and the NG15 team, <https://zenodo.org/records/10344086>.
- [62] G. Agazie *et al.* [NANOGrav], “The NANOGrav 15 yr Data Set: Observations and Timing of 68 Millisecond Pulsars,” *Astrophys. J. Lett.* **951**, no.1, L9 (2023) [arXiv:2306.16217 [astro-ph.HE]].
- [63] Antoniadis, J., Arumugam, P., and the EPTA DR2 team, <https://zenodo.org/records/8091568>.
- [64] J. Antoniadis *et al.* [EPTA], “The second data release from the European Pulsar Timing Array - I. The dataset and timing analysis,” *Astron. Astrophys.* **678**, A48 (2023) [arXiv:2306.16224 [astro-ph.HE]].
- [65] Zic, Andrew; Reardon, Daniel John; and the PPTA DR3 team, <https://doi.org/10.25919/j4xr-wp05>.
- [66] A. Zic, D. J. Reardon, A. Kapur, G. Hobbs, R. Mandow, M. Curyło, R. M. Shannon, J. Askew, M. Bailes and N. D. R. Bhat, *et al.* “The Parkes Pulsar Timing Array third data release,” *Publ. Astron. Soc. Austral.* **40**, e049 (2023) [arXiv:2306.16230 [astro-ph.HE]].
- [67] International Pulsar Timing Array Collaboration, <https://zenodo.org/records/5787557>.
- [68] B. B. P. Perera, M. E. DeCesar, P. B. Demorest, M. Kerr, L. Lentati, D. J. Nice, S. Osłowski, S. M. Ransom, M. J. Keith and Z. Arzoumanian, *et al.* “The International Pulsar Timing Array: Second data release,” *Mon. Not. Roy. Astron. Soc.* **490**, no.4, 4666-4687 (2019) [arXiv:1909.04534 [astro-ph.HE]].
- [69] P. A. Rosado, A. Sesana and J. Gair, “Expected properties of the first gravitational wave signal detected with pulsar timing arrays,” *Mon. Not. Roy. Astron. Soc.* **451**, no.3, 2417-2433 (2015) [arXiv:1503.04803 [astro-ph.HE]].
- [70] M. Benetti, L. L. Graef and S. Vagnozzi, “Primordial gravitational waves from NANOGrav: A broken power-law approach,” *Phys. Rev. D* **105**, no.4, 043520 (2022) [arXiv:2111.04758 [astro-ph.CO]].
- [71] Y. K. E. Cheung, C. Li and J. D. Vergados, “Big Bounce Genesis and Possible Experimental Tests: A Brief Review,” *Symmetry* **8**, no.11, 136 (2016) [arXiv:1611.04027 [astro-ph.CO]].
- [72] A. Mitridate, D. Wright, R. von Eckardstein, T. Schröder, J. Nay, K. Olum, K. Schmitz and T. Trickle, [arXiv:2306.16377 [hep-ph]].
- [73] W. G. Lamb, S. R. Taylor and R. van Haasteren, *Phys. Rev. D* **108**, no.10, 103019 (2023) [arXiv:2303.15442 [astro-ph.HE]].
- [74] J. Buchner, “Nested sampling methods,” [arXiv:2101.09675 [stat.CO]].
- [75] Justin Ellis, Rutger van Haasteren, <https://doi.org/10.5281/zenodo.1037579>.
- [76] C. F. Chang and Y. Cui, “Gravitational waves from global cosmic strings and cosmic archaeology,” *JHEP* **03**, 114 (2022) [arXiv:2106.09746 [hep-ph]].
- [77] K. Kadota, M. Kawasaki and K. Saikawa, “Gravitational waves from domain walls in the next-to-minimal supersymmetric standard model,” *JCAP* **10**, 041 (2015) [arXiv:1503.06998 [hep-ph]].
- [78] R. Zhou, J. Yang and L. Bian, “Gravitational Waves from first-order phase transition and domain wall,” *JHEP* **04**, 071 (2020) [arXiv:2001.04741 [hep-ph]].
- [79] T. Hirose and H. Shibuya, “Relation between higher-dimensional gauge theories and gravitational waves from first-order phase transitions,” *Phys. Rev. D* **109**, no.7, 075013 (2024) [arXiv:2303.14192 [hep-ph]].
- [80] A. H. Guth, “The Inflationary Universe: A Possible Solution to the Horizon and Flatness Problems,” *Phys. Rev. D* **23** (1981), 347-356
- [81] A. A. Starobinsky, “A New Type of Isotropic Cosmological Models Without Singularity,” *Phys. Lett. B* **91**, 99-102 (1980)
- [82] K. Sato, “First Order Phase Transition of a Vacuum and Expansion of the Universe,” *Mon. Not. Roy. Astron. Soc.* **195**, 467-479 (1981) NORDITA-80-29.
- [83] A. D. Linde, “A New Inflationary Universe Scenario: A Possible Solution of the Horizon, Flatness, Homogeneity, Isotropy and Primordial Monopole Problems,” *Phys. Lett. B* **108**, 389-393 (1982)
- [84] A. Albrecht and P. J. Steinhardt, “Cosmology for Grand Unified Theories with Radiatively Induced Symmetry Breaking,” *Phys. Rev. Lett.* **48**, 1220-1223 (1982)
- [85] V. F. Mukhanov, H. A. Feldman and R. H. Brandenberger, “Theory of cosmological perturbations. Part 1. Classical perturbations. Part 2. Quantum theory of perturbations. Part 3. Extensions,” *Phys. Rept.* **215**, 203-333 (1992)
- [86] A. Borde and A. Vilenkin, “Eternal inflation and the initial singularity,” *Phys. Rev. Lett.* **72**, 3305-3309 (1994) [arXiv:gr-qc/9312022 [gr-qc]].
- [87] M. Gasperini and G. Veneziano, *Phys. Rept.* **373**, 1-212 (2003) [arXiv:hep-th/0207130 [hep-th]].
- [88] P. Creminelli, M. A. Luty, A. Nicolis and L. Senatore, *JHEP* **12**, 080 (2006) [arXiv:hep-th/0606090 [hep-th]].
- [89] P. Peter, E. J. C. Pinho and N. Pinto-Neto, *Phys. Rev. D* **75**, 023516 (2007) [arXiv:hep-th/0610205 [hep-th]].
- [90] Y. F. Cai, T. Qiu, Y. S. Piao, M. Li and X. Zhang, *JHEP* **10**, 071 (2007) [arXiv:0704.1090 [gr-qc]].
- [91] Y. F. Cai, T. t. Qiu, R. Brandenberger and X. m. Zhang, *Phys. Rev. D* **80**, 023511 (2009) [arXiv:0810.4677 [hep-th]].
- [92] T. Saitov and A. Zhuk, *Phys. Rev. D* **81**, 124002 (2010) [arXiv:1002.4138 [hep-th]].
- [93] Y. F. Cai, S. H. Chen, J. B. Dent, S. Dutta and E. N. Saridakis, *Class. Quant. Grav.* **28**, 215011 (2011) [arXiv:1104.4349 [astro-ph.CO]].
- [94] D. A. Easson, I. Sawicki and A. Vikman, *JCAP* **11**, 021 (2011) [arXiv:1109.1047 [hep-th]].
- [95] K. Bhattacharya, Y. F. Cai and S. Das, *Phys. Rev. D* **87**, no.8, 083511 (2013) [arXiv:1301.0661 [hep-th]].
- [96] T. Qiu and Y. T. Wang, *JHEP* **04**, 130 (2015) [arXiv:1501.03568 [astro-ph.CO]].
- [97] Y. F. Cai, A. Marciano, D. G. Wang and E. Wilson-Ewing, *Universe* **3**, no.1, 1 (2016) [arXiv:1610.00938 [astro-ph.CO]].
- [98] J. D. Barrow and C. Ganguly, *Phys. Rev. D* **95**, no.8, 083515 (2017) [arXiv:1703.05969 [gr-qc]].
- [99] J. De Haro and J. Amorós, *Phys. Rev. D* **97**, no.6, 064014 (2018) [arXiv:1712.08399 [gr-qc]].
- [100] A. Ijjas and P. J. Steinhardt, *Class. Quant. Grav.* **35**, no.13, 135004 (2018) [arXiv:1803.01961 [astro-ph.CO]].
- [101] S. S. Boruah, H. J. Kim, M. Rouben and G. Geshnizjani, *JCAP* **08**, 031 (2018) [arXiv:1802.06818 [gr-qc]].
- [102] S. Nojiri, S. D. Odintsov and E. N. Saridakis, *Nucl. Phys. B* **949**, 114790 (2019) [arXiv:1908.00389 [gr-qc]].

- [103] C. Li, R. H. Brandenberger and Y. K. E. Cheung, “Big-Bounce Genesis,” *Phys. Rev. D* **90**, no.12, 123535 (2014) [arXiv:1403.5625 [gr-qc]].
- [104] Y. K. E. Cheung, J. U. Kang and C. Li, “Dark matter in a bouncing universe,” *JCAP* **11**, 001 (2014) [arXiv:1408.4387 [astro-ph.CO]].
- [105] C. Li, “Thermally producing and weakly freezing out dark matter in a bouncing universe,” *Phys. Rev. D* **92**, no.6, 063513 (2015) [arXiv:1404.4012 [astro-ph.CO]].
- [106] C. Li, “Thermal Fluctuations of Dark Matter in Bouncing Cosmology,” *JCAP* **09**, 038 (2016) [arXiv:1512.06794 [astro-ph.CO]].
- [107] C. Li, “Warm and Cold Dark Matter in Bouncing Universe,” *Phys. Rev. D* **102**, 123530 (2020) [arXiv:2008.10264 [astro-ph.CO]].
- [108] M. Novello and S. E. P. Bergliaffa, *Phys. Rept.* **463**, 127-213 (2008) [arXiv:0802.1634 [astro-ph]].
- [109] R. Brandenberger and P. Peter, *Found. Phys.* **47**, no.6, 797-850 (2017) [arXiv:1603.05834 [hep-th]].
- [110] S. Nojiri, S. D. Odintsov and V. K. Oikonomou, “Modified Gravity Theories on a Nutshell: Inflation, Bounce and Late-time Evolution,” *Phys. Rept.* **692**, 1-104 (2017) [arXiv:1705.11098 [gr-qc]].
- [111] Y. F. Cai, E. N. Saridakis, M. R. Setare and J. Q. Xia, “Quintom Cosmology: Theoretical implications and observations,” *Phys. Rept.* **493**, 1-60 (2010) [arXiv:0909.2776 [hep-th]].

### Supplemental Material: Dual Inflation and Bounce Cosmologies Interpretation of Pulsar Timing Array Data

This supplemental material contains additional details on: A. the dual scenario of generalized inflation and bounce cosmologies, as previously outlined in Ref. [54]; B. the SGWB spectrum, prior and posterior distributions of each model; C. the data analysis methodology and Bayes factor (BF) matrices for all model comparisons; and D. the results pertaining to the nearly scale-invariant case ( $n_s - 1 = -0.04$ )[43–45].

### Dual Scenario of Generalized Inflation and Bounce Cosmologies

This section provides a concise introduction to the dual scenario of generalized inflation and bounce cosmologies. The calculations of curvature perturbations follow the methodology outlined in Ref. [54].

The standard single-field slow-roll inflation, renowned for resolving early universe challenges like the flatness and horizon problems [80–85], generates a nearly scale-invariant primordial curvature perturbation spectrum consistent with current cosmic microwave background (CMB) observations [43–45]. However, it faces the initial singularity problem, which undermines its physical basis [86]. Bounce cosmology offers a compelling alternative by naturally circumventing this singularity, starting with a contracting phase before transitioning to expansion through a bounce process [50, 59, 87–102]. Bounce models can also produce a nearly scale-invariant primordial curvature perturbation spectrum and may address concerns such as dark matter abundance [103–106] and the small-scale crisis [107]. Thus, both inflation and bounce models warrant further investigation and development in cosmology and astrophysics; see [108–110] for a comprehensive review.

Despite the disparate cosmic evolution trajectories of inflationary and bouncing universe models (each phase is summarized in Table III), they exhibit strikingly similar patterns in generating curvature perturbations, as depicted in Fig.3 (cf. Fig. 1 in Ref.[71]). This observation prompted their integration into a unified parameter space, a concept pioneered by David Wands in Ref.[55] and by Fabio Finelli and Robert Brandenberger in Ref.[56], recognized as Wands’s duality. In particular, Wands’s duality is symbolized by the horizontal HT arrow in Fig.4 (cf. Fig. 2 in Ref.[54]). Noting that such duality is established by extending the conventional Hubble radius  $\mathcal{H}^{-1} \equiv (aH)^{-1}$ , used only for inflation, to the “effective” Hubble radius  $\mathcal{H}_u^{-1} \equiv |aH|^{-1}$ , where  $a$  and  $H$  are the scale factor and Hubble parameter, respectively.

TABLE III. Each phase in inflation and bounce cosmologies

	Case	$\dot{a}$	$\ddot{a}$	$\omega$	$\nu$	$k\eta$	Example
Inflation	Accelerating expansion	$> 0$	$> 0$	$< -1/3$	$< 0$	$\rightarrow 0$	Slow-roll inflation
	Decelerating expansion	$> 0$	$< 0$	$> -1/3$	$> 0$	$\rightarrow \infty$	Post-BBN universe
Bounce	Collapsing contraction	$< 0$	$< 0$	$> -1/3$	$> 0$	$\rightarrow 0$	Matter dominated
	Bouncing contraction	$< 0$	$> 0$	$< -1/3$	$< 0$	$\rightarrow \infty$	Quintom dominated [111]
	Bouncing expansion	$> 0$	$> 0$	$< -1/3$	$< 0$	$\rightarrow 0$	Quintom dominated [111]
	Decelerating expansion	$> 0$	$< 0$	$> -1/3$	$> 0$	$\rightarrow \infty$	Post-BBN universe

Wands’s duality provides a theoretical foundation for model-building in bounce cosmologies to generate a scale-invariant curvature perturbation spectrum, as seen in matter bounce models, which have achieved significant success. However, the scale-invariant curvature spectrum from Wands’s duality is time-dependent,  $\mathcal{P}_{\mathcal{R}} \propto k^0 \eta^{-4\nu+2}$ . For instance, in the matter bounce model ( $\nu = 2$ ), one has  $\mathcal{P}_{\mathcal{R}} \propto k^0 \eta^{-6}$ , which does not perfectly correspond to the time-independent case for inflation,



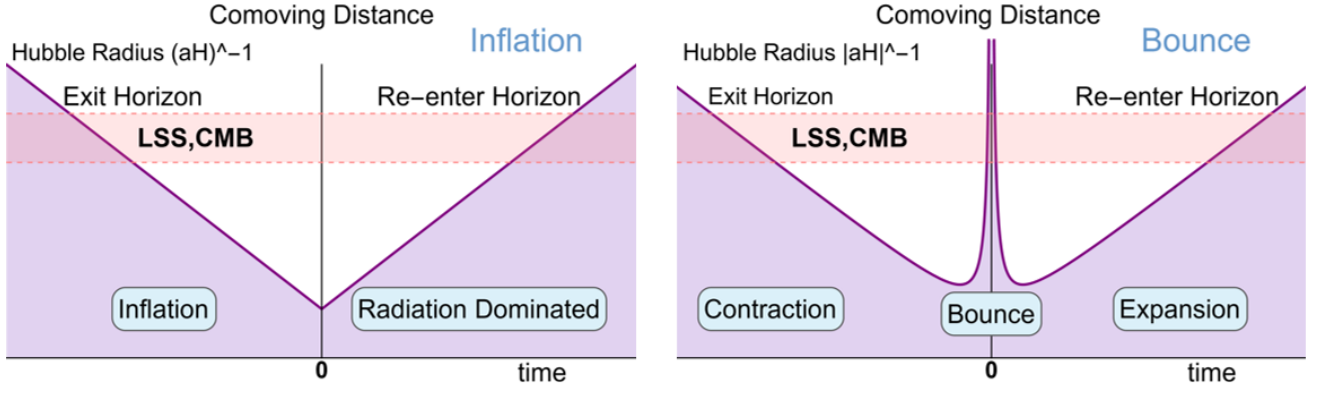


FIG. 3. Left: Evolution of the Hubble radius  $((aH)^{-1})$  in the inflationary scenario. Curvature perturbation modes (horizontal pink region) exit the horizon (solid purple lines) during accelerating expansion and re-enter during decelerating expansion. Right: Evolution of the "effective" Hubble radius  $(|aH|^{-1})$  in the bounce scenario, resembling the inflationary scenario. Modes exit during collapsing contraction, transition through the bounce region, and re-enter during decelerating expansion.

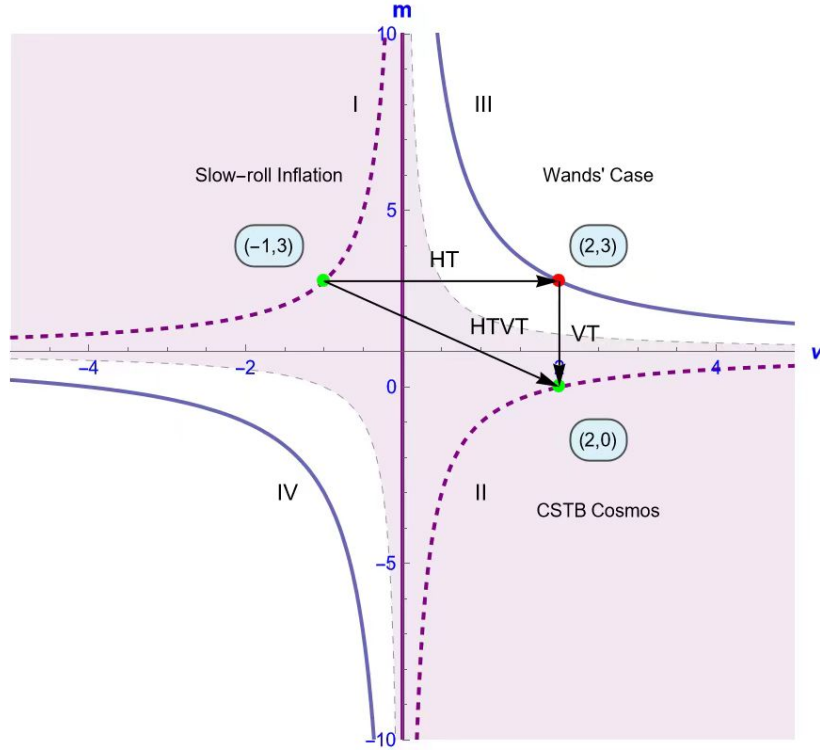


FIG. 4. The parameter space  $(m, \nu)$  for the scenario of generalized inflation and bounce cosmologies. The shaded region represents the range within which the time-independent (stable) curvature perturbation spectrum can be generated. The dashed curves represent the stable scale-invariant solutions for inflation (bottom left) and bounce (bottom right) cosmologies, while the solid curves represent the dynamic scale-invariant solutions for inflation (bottom left) and bounce (top right).

$\mathcal{P}_{\mathcal{R}} \propto k^0 \eta^0$ . Here,  $\mathcal{P}_{\mathcal{R}}$  is the power spectrum of curvature perturbations,  $k$  is the wave-vector of curvature perturbation modes,  $\eta$  is the conformal time, and  $\nu$  is the power-law index of the scale factor,  $a(\eta) \propto \eta^\nu$ .

To find a time-independent scale-invariant solution in bounce cosmologies, akin to standard inflation, and to accommodate various generalized models of inflation and bounce cosmologies, the redshift term coefficient of curvature perturbation modes  $\chi_k$  was phenomenologically generalized from  $3H$  to  $mH$ , leading to (cf. Eq.(4.1) in Ref. [54]):

$$\ddot{\chi}_k + mH\dot{\chi}_k + \frac{k^2}{a^2}\chi_k = 0, \quad a(\eta) \propto \eta^\nu, \quad (7)$$

where  $m$  is assumed to be a constant varying with the specific generalization of inflation and bounce cosmology models, characterizing various levels of damping behavior, from enhanced to suppressed effects. For instance,  $m = 3$  for standard inflation, whereas  $m = 0$  for the coupled scalar tachyon bounce (CSTB) universe model.

Due to the extension of the Hubble radius and the phenomenological generalization of the redshift term for curvature perturbations, various inflation and bounce cosmologies are unified into a single parameter space,  $(\nu, m)$ , as illustrated in Fig.4, offering new insights for the investigation of the early universe and the model-building of inflation or bounce phases. Specifically, in Fig.4, the shaded region represents time-independent (stable) solutions. The horizontal transformation (HT) (e.g., Wands's duality) denotes iso-damping duality with the same  $m$ , while the vertical transformation (VT) represents iso-temporal duality with the same  $\nu$ . The combination of these transformations, HTVT, is a duality connecting stable scale-invariant solutions from inflationary and bouncing cosmologies, such as standard inflation and CSTB cosmologies.

Within the parameter space  $(m, \nu)$ , by solving Eq.(7), one can obtain the leading-order power spectrum of primordial curvature perturbation outside the "effective" horizon,  $k\eta \rightarrow 0$ , as (cf. Eq.(4.2) in Ref. [54]):

$$\mathcal{P}_{\mathcal{R}} \equiv \frac{k^3 |\chi_k|^2}{2\pi^2} \propto k^{2L(m,\nu)+3} \eta^{2W(m,\nu)}, \quad (8)$$

where the indices  $L$  and  $W$  are functions of  $m$  and  $\nu$ :

$$L(m, \nu) = -\frac{1}{2}|(m-1)\nu - 1|, \quad W(m, \nu) = -\frac{1}{2}[(m-1)\nu - 1 + |(m-1)\nu - 1|]. \quad (9)$$

Using Eq.(8) and Eq.(9), one can identify the time-independent region,  $2W(m, \nu) = 0$ , within the  $(\nu, m)$  parameter space:

$$(m-1)\nu - 1 < 0, \quad (10)$$

as illustrated by the shaded region in Fig.4 (cf. Fig. 3 in Ref.[54]). Furthermore, according to Eq. (8), the power spectrum index of curvature perturbation,  $\mathcal{P}_{\mathcal{R}} \propto k^{n_s-1}$ , is given by  $n_s - 1 = 2L(m, \nu) + 3$ . Using the scale-invariance condition,  $n_s - 1 = 0$ , we have:

$$n_s - 1 = 2L(m, \nu) + 3 = 0. \quad (11)$$

Solving Eq.(11), we obtain two groups of scale-invariant solutions: one is the time-independent (stable) scale-invariant solution, depicted as dashed curves within the time-independent region in Fig.4:

$$m = -\frac{2}{\nu} + 1, \quad (12)$$

and the other is the time-dependent (dynamic) scale-invariant solution, depicted as solid curves outside the time-independent region in Fig. 4:

$$m = \frac{4}{\nu} + 1. \quad (13)$$

In these two solutions, the damping parameter  $m$ , which characterizes the enhanced or suppressed damping effect, balances the power index of the scale factor  $\nu$ , which characterizes the temporal effect from the cosmic background, to generate scale-invariant curvature perturbation spectra. As illustrated in Fig. 4, the models that can generate a scale-invariant curvature perturbation spectrum, including standard inflation, Wands's case (Matter bounce), and CSTB cosmos, are located on these two groups of solutions.

**Primordial Gravitational Waves** – In the dual scenario, the coefficient of the redshift term for tensor modes ( $3H$ ) is not modified, in contrast to the generalized redshift term  $mH$  for curvature perturbations. Consequently, their spectral indices,  $n_T$  and  $n_s - 1$ , can be significantly different. In Fourier space, the equation of motion for the tensor mode is given by:

$$H_r''(\mathbf{k}, \eta) + \left(k^2 - \frac{a''}{a}\right) H_r(\mathbf{k}, \eta) = 0, \quad (14)$$

where  $H_r(\mathbf{k}, \eta) \equiv a(\eta)h_r(\mathbf{k}, \eta)$ ,  $h_r$  denotes the tensor part of the metric perturbation ( $h_+$  and  $h_\times$ ), and the superscript  $'$  denotes derivatives with respect to the conformal time  $\eta$ ,  $d\eta = dt/a(t)$ .

Solving Eq. (14) with  $a(\eta) \propto \eta^\nu$  for the leading order term in the limit  $k\eta \rightarrow 0$ , one can obtain the power spectrum of tensor modes,

$$\mathcal{P}_h \equiv \frac{k^3 |h_r|^2}{2\pi^2} \propto k^{-|2\nu-1|+3} \eta^{-[2\nu-1+|2\nu-1|]}. \quad (15)$$

The spectral index of tensor modes ( $\mathcal{P}_h \propto k^{n_T}$ ) is measured when they re-enter the horizon ( $k\eta = 1$ ) at the pivot scale  $k_* = 0.05$  Mpc, which leads to

$$\mathcal{P}_h \propto k^{-|2\nu-1|+3} (k^{-1})^{-[2\nu-1+|2\nu-1|]} \propto k^{2\nu+2}, \quad (16)$$

and reproduces  $n_T = 2\nu + 2$ . Using  $a(\eta) \propto \eta^{\frac{2}{3w+1}}$  obtained by solving the Friedmann equation, which indicates  $\nu = \frac{2}{3w+1}$ , we re-obtain  $n_T = \frac{4}{3w+1} + 2$ . Using Eq.(12) and Eq.(16), we reproduce the well-known result for standard inflation ( $(m, \nu) = (3, -1)$ ),  $n_s - 1 = 0$  and  $n_T = 0$ , in this dual scenario description.

### SGWB spectrum, Prior and Posterior Distributions of Each Model

This section provides a summary of the stochastic gravitational wave background (SGWB) spectrum and the prior and posterior distributions for each model discussed in the main text.

1. Model-1: The dual scenario of generalized inflation and bounce cosmologies in terms of the parameter space  $(n_T, r)$ , specifically described by Eq. (2). The SGWB spectrum of this model is given by:

$$\Omega_{\text{GW}}(f)h^2 = \frac{3}{128}\Omega_{\gamma_0}h^2 \cdot r \cdot \mathcal{P}_{\mathcal{R}} \left( \frac{f}{f_*} \right)^{n_T} \left[ \frac{1}{2} \left( \frac{f_{\text{eq}}}{f} \right)^2 + \frac{16}{9} \right]. \quad (17)$$

Here,  $r$  and  $n_T$  denote, respectively, the tensor-to-scalar ratio ( $r \equiv \mathcal{P}_h/\mathcal{P}_{\mathcal{R}}$ ) and the spectral index of the primordial tensor spectrum at the pivot scale  $k_* = 0.05\text{Mpc}^{-1}$ .  $\mathcal{P}_{\mathcal{R}} = 2 \times 10^{-9}$  is the amplitude of the curvature perturbation spectrum at  $k_*$  [9]. Additionally,  $f_* = 1.55 \times 10^{-15}\text{Hz}$  corresponds to the frequency today for  $k_*$ , while  $f_{\text{eq}} = 2.01 \times 10^{-17}\text{Hz}$  represents the frequency today at matter-radiation equality.  $\Omega_{\gamma_0} = 2.474 \times 10^{-5}h^{-2}$  is the energy density fraction of radiation today, where  $h = 0.6770$  is the reduced Hubble constant.

2. Model-2: The dual scenario of generalized inflation and bounce cosmologies in terms of the parameter space  $(w, r)$ , utilizing the equation  $n_T = \frac{4}{3w+1} + 2$  for  $w \in (-\infty, \infty)$ , specifically described by Eq.(3). The SGWB spectrum of this model is given by

$$\Omega_{\text{GW}}(f)h^2 = \frac{3}{128}\Omega_{\gamma_0}h^2 \cdot r \cdot \mathcal{P}_{\mathcal{R}} \left( \frac{f}{f_*} \right)^{\left[\frac{4}{3w+1}+2\right]} \left[ \frac{1}{2} \left( \frac{f_{\text{eq}}}{f} \right)^2 + \frac{16}{9} \right]. \quad (18)$$

3. Model-3: The time-independent (stable) scale-invariant solution of the dual scenario in terms of parameter space  $(m, r)$ , utilizing the  $m = -\frac{2}{\nu} + 1$  for  $m \in (-\infty, \infty)$ , specifically described by Eq.(5). The SGWB spectrum of this model is given by

$$\Omega_{\text{GW}}(f)h^2 = \frac{3}{128}\Omega_{\gamma_0}h^2 \cdot r \cdot \mathcal{P}_{\mathcal{R}} \left( \frac{f}{f_*} \right)^{\left[-\frac{4}{m-1}+2\right]} \left[ \frac{1}{2} \left( \frac{f_{\text{eq}}}{f} \right)^2 + \frac{16}{9} \right]. \quad (19)$$

4. Model-4: The time-dependent (dynamic) scale-invariant solution of the dual scenario in terms of parameter space  $(m, r)$ , utilizing the  $m = \frac{4}{\nu} + 1$  for  $m \in (-\infty, \infty)$ , specifically described by Eq.(6). The SGWB spectrum of this model is given by

$$\Omega_{\text{GW}}(f)h^2 = \frac{3}{128}\Omega_{\gamma_0}h^2 \cdot r \cdot \mathcal{P}_{\mathcal{R}} \left( \frac{f}{f_*} \right)^{\left[\frac{8}{m-1}+2\right]} \left[ \frac{1}{2} \left( \frac{f_{\text{eq}}}{f} \right)^2 + \frac{16}{9} \right]. \quad (20)$$

5. Model-5: The time-independent (stable) **nearly** scale-invariant solution of the dual scenario in terms of parameter space  $(m, r)$ , utilizing the  $m = -\frac{2-(n_s-1)}{\nu} + 1$  for  $m \in (-\infty, \infty)$  and  $n_s - 1 = -0.04$ . The SGWB spectrum of this model is given by

$$\Omega_{\text{GW}}(f)h^2 = \frac{3}{128}\Omega_{\gamma_0}h^2 \cdot r \cdot \mathcal{P}_{\mathcal{R}} \left( \frac{f}{f_*} \right)^{\left[-\frac{4.08}{m-1}+2\right]} \left[ \frac{1}{2} \left( \frac{f_{\text{eq}}}{f} \right)^2 + \frac{16}{9} \right]. \quad (21)$$

6. Model-6: The time-dependent (dynamic) **nearly** scale-invariant solution of the dual scenario in terms of parameter space  $(m, r)$ , utilizing the  $m = \frac{4+(n_s-1)}{\nu} + 1$  for  $m \in (-\infty, \infty)$  and  $n_s - 1 = -0.04$ . The SGWB spectrum of this model is given by

$$\Omega_{\text{GW}}(f)h^2 = \frac{3}{128}\Omega_{\gamma_0}h^2 \cdot r \cdot \mathcal{P}_{\mathcal{R}} \left( \frac{f}{f_*} \right)^{\left[ \frac{7.92}{m-1} + 2 \right]} \left[ \frac{1}{2} \left( \frac{f_{\text{eq}}}{f} \right)^2 + \frac{16}{9} \right]. \quad (22)$$

7. Model-7: Supermassive black hole binaries (SMBH binaries). The SGWB spectrum of this model is given by [22]

$$\Omega_{\text{GW}}^{\text{SMBHB}}(f)h^2 = A_{\text{SMBHB}}^2 \frac{2\pi^2}{3H_0^2} f^{5-\gamma} f_{\text{yr}}^{3-\gamma} h^2. \quad (23)$$

Here  $\gamma = 13/3, A_{\text{SMBHB}}$  is the Amplitude of SGWB.

8. Model-8: Cosmic strings (CS). The SGWB spectrum of this model is given by [31]

$$\Omega_{\text{GW}}^{\text{CS}}(f)h^2 = \frac{8\pi}{3H_0^2} (G\mu)^2 \sum_{k=1}^{k_{\text{max}}} P_k \mathcal{I}_k(f)h^2 \quad (24)$$

The prior parameter  $G\mu$ , a dimensionless factor, denotes the tension of cosmic strings in units of Newton's constant. The dimensionless factor  $P_k$  represents the power of gravitational waves emitted by a loop in its  $k$ -th excitation and  $\mathcal{I}_k(f)$  is the frequency-dependent factor.

9. Model-9: Domain walls (DW). The SGWB spectrum of this model is given by [76–78]

$$\Omega_{\text{GW}}^{\text{DW}}(f)h^2 = \Omega_{\text{GW}}^{\text{peak}} h^2 S^{\text{dw}}(f) \quad (25)$$

where the peak GW amplitude is

$$\Omega_{\text{GW}}^{\text{peak}} h^2 \simeq 5.20 \times 10^{-20} \times \tilde{\epsilon}_{\text{gw}} \mathcal{A}^4 \left( \frac{10.75}{g_*} \right)^{1/3} \times \left( \frac{\sigma}{1\text{TeV}^3} \right)^4 \left( \frac{1\text{MeV}^4}{\Delta V} \right)^2 \quad (26)$$

and the shape function  $S^{\text{dw}}(f)$  is

$$\begin{aligned} S^{\text{dw}}(f) &= (f/f_{\text{peak}}^{\text{dw}})^3, & f < f_{\text{peak}}^{\text{dw}} \\ S^{\text{dw}}(f) &= (f/f_{\text{peak}}^{\text{dw}})^{-1}, & f \geq f_{\text{peak}}^{\text{dw}} \end{aligned} \quad (27)$$

where the peak frequency is [76]

$$f_{\text{peak}}^{\text{dw}} \simeq 3.99 \times 10^{-9} \text{ Hz} \mathcal{A}^{-\frac{1}{2}} \left( \frac{1\text{TeV}^3}{\sigma} \right)^{\frac{1}{2}} \left( \frac{\Delta V}{1\text{MeV}^4} \right)^{\frac{1}{2}} \quad (28)$$

Here, the prior parameters  $\sigma$  and  $\Delta V$  respectively represent the tension of the domain wall and the bias potential that breaks the degeneracy of the vacua. The bias potential leads to the disappearance of the domain wall and marks the location of the peak frequency.  $\mathcal{A} = 1.2$ [76, 77] is the area parameter.  $\tilde{\epsilon}_{\text{gw}} = 0.7$ [76] is the efficiency parameter for generating gravitational waves.

10. Model-10: First-order phase transitions (FOPT). The SGWB spectrum of this model is given by[26, 33]

$$\begin{aligned} \Omega_{\text{GW}}^{\text{FOPT}}(f)h^2 &= 2.65 \times 10^{-6} (H_* \tau_{\text{sw}}) \left( \frac{\beta}{H_*} \right)^{-1} v_b \left( \frac{\kappa_v \alpha_{PT}}{1 + \alpha_{PT}} \right)^2 \\ &\times \left( \frac{g_*}{100} \right)^{-\frac{1}{3}} \left( \frac{f}{f_{\text{peak}}^{\text{sw}}} \right)^3 \left[ \frac{7}{4 + 3 \left( f/f_{\text{peak}}^{\text{sw}} \right)^2} \right]^{7/2}, \end{aligned} \quad (29)$$

with the peak frequency

$$f_{\text{peak}}^{\text{FOPT}} = 1.9 \times 10^{-5} \frac{\beta}{H_*} \frac{1}{v_b} \frac{T_*}{100} \left( \frac{g_*}{100} \right)^{\frac{1}{6}} \text{ Hz.} \quad (30)$$

Here,  $\tau_{\text{sw}} = \min \left[ \frac{1}{H_*}, \frac{R_s}{v_b} \right]$  denotes the duration of the sound wave phase.  $H_*$  is the Hubble parameter at temperature  $T_*$ . The proportion of vacuum energy allocated to each source, denoted as  $\kappa_\nu$  [78, 79], is related to  $\alpha_{PT}$ , which represents the latent heat. Additionally,  $\beta/H_n$  corresponds to the inverse duration of the phase transition,  $v_b$  denotes the velocity of the vacuum bubble wall in the plasma background.  $g_*$  is the effective number of degrees of freedom for relativistic particles in the cosmic plasma at the time of gravitational wave formation.

11. Model-11: Scalar-induced gravitational waves (SIGW). The SGWB spectrum of this model is given by[30]

$$\begin{aligned} \Omega_{\text{GW}}^{\text{SI}}(f)h^2 &= \frac{1}{12} \Omega_{\text{rad}} h^2 \left( \frac{g_0}{g_*} \right)^{\frac{1}{3}} \times \int_0^\infty dv \int_{|1-v|}^{1+v} du \left( \frac{4v^2 - (1+v^2-u^2)^2}{4uv} \right)^2 \\ &\times P_{\mathcal{R}}(2\pi fu) P_{\mathcal{R}}(2\pi fv) I^2(u, v), \end{aligned} \quad (31)$$

where

$$\begin{aligned} I^2(u, v) &= \frac{1}{2} \left( \frac{3}{4u^3 v^3 x} \right)^2 (u^2 + v^2 - 3)^2 \\ &\times \left\{ \left[ -4uv + (u^2 + v^2 - 3) \ln \left| \frac{3 - (u+v)^2}{3 - (u-v)^2} \right| \right]^2 \right. \\ &\left. + \left[ \pi (u^2 + v^2 - 3) \Theta(u + v - \sqrt{3}) \right]^2 \right\}. \end{aligned} \quad (32)$$

Here,  $P_{\mathcal{R}}(k)$  represents the power spectrum of curvature perturbations. We consider a scenario where  $P_{\mathcal{R}}(k)$  adopts a power-law form near  $k = 2\pi f_* = 20.6 \text{ pc}^{-1}$ , with  $f_* = 1 \text{ yr}^{-1}$

$$P_{\mathcal{R}}(k) = P_{\mathcal{R}0} \left( \frac{k}{k_*} \right)^n \Theta(k - k_{\min}) \Theta(k_{\max} - k), \quad (33)$$

where  $\Theta(x)$  is the Heaviside function,  $P_{\mathcal{R}0}$  is the power spectrum of scalar perturbations at  $k = k_*$ ,  $n$  represents the slope of the power spectrum for scalar perturbations. To prevent an excessive production of primordial black holes (PBHs), cutoffs are set at  $k_{\min} = 0.03k_*$  and  $k_{\max} = 100k_*$ , imposing an upper limit on  $P_{\mathcal{R}}(k)$ [33].

In Table.IV, we assign uniform or log-uniform priors to all parameters for each model, which are utilized for Bayesian analysis in this work.

### Data analysis methodology and Bayes factor (BF) matrices

In our Bayesian analysis, we employed Ceffyl [73] to fit Model-1 to Model-11, as listed in Tab. IV in Section , within their respective prior ranges specified in Table IV, using data from NANOGrav 15-year [2, 31, 61, 62], EPTA DR2[4, 63, 64], PPTA DR3[6, 65, 66], and IPTA DR2[7, 67, 68] datasets. Specifically, we utilized the PTMCMC sampler in Ceffyl to generate the posterior distribution for each case and UltraNest in Ceffyl to compute the Bayes Factors for each case, as listed in as listed in Tab. V-Tab. VII and Eq.(34)-Eq.(37). In particular, in Eq.(34)-Eq.(37), the Bayes factor (BF) matrices,  $B_{ij} = \text{evidence}[H_i]/\text{evidence}[H_j]$ , are organized in the order  $i, j = \text{SMBHBs, CS, DW, FOPT, and SIGW}$ . The Bayes factor matrices for the conventional sources are consistent with previous results in [31, 33]

$$B_{ij}^{\text{NG15}} = \begin{pmatrix} 1.0 & 4.8 \pm 1.9 & 3.4 \pm 1.2 & 0.7 \pm 0.2 & 4.0 \pm 1.1 \\ 0.2 \pm 0.1 & 1.0 & 0.7 \pm 0.2 & 0.1 \pm 0.03 & 0.1 \pm 0.03 \\ 0.3 \pm 0.1 & 1.4 \pm 0.4 & 1.0 & 0.2 \pm 0.04 & 0.2 \pm 0.04 \\ 1.5 \pm 0.5 & 7.4 \pm 1.8 & 5.3 \pm 1.0 & 1.0 & 1.1 \pm 0.2 \\ 1.4 \pm 0.4 & 7.0 \pm 1.5 & 4.9 \pm 0.9 & 0.9 \pm 0.2 & 1.0 \end{pmatrix} \quad (34)$$

TABLE IV. Summary of all priors

Parameter	Description	Prior
<b>Model-1: Dual scenario</b> ( $n_T, r$ )		
$n_T$	Spectral index of tensor spectrum	uniform $[-1, 6]$
$r$	Tensor-to-scalar ratio	log-uniform $[-16, 0]$
<b>Model-2: Dual scenario</b> ( $w, r$ )		
$w$	Equation of state	uniform $[-10, 10]$
$r$	Tensor-to-scalar ratio	log-uniform $[-16, 0]$
<b>Model-3: Stable Scale-invariant</b> ( $m, r$ )		
$m$	Stable scale-invariant factor	uniform $[-32, 32]$
$r$	Tensor-to-scalar ratio	log-uniform $[-16, 0]$
<b>Model-4: Dynamic Scale-invariant</b> ( $m, r$ )		
$m$	Dynamic scale-invariant factor	uniform $[-32, 32]$
$r$	Tensor-to-scalar ratio	log-uniform $[-16, 0]$
<b>Model-5: Stable nearly Scale-invariant</b> ( $m, r$ )		
$m$	Stable nearly scale-invariant factor	uniform $[-32, 32]$
$r$	Tensor-to-scalar ratio	log-uniform $[-16, 0]$
<b>Model-6: Dynamic nearly Scale-invariant</b> ( $m, r$ )		
$m$	Dynamic nearly scale-invariant factor	uniform $[-32, 32]$
$r$	Tensor-to-scalar ratio	log-uniform $[-16, 0]$
<b>Model-7:SMBHBs (PL <math>n_t = 13/3</math>)</b>		
$A_{\text{SMBHB}}$	Amplitude of the signal	log-uniform $[-18, -12]$
<b>Model-8:CS</b>		
$G\mu$	Cosmic-string tension	log-uniform $[-12, -6]$
<b>Model-9:DW</b>		
$\sigma$	Surface energy density	log-uniform $[0, 8]$
$\Delta V$	Bias potential	log-uniform $[0, 8]$
<b>Model-10:FOPT</b>		
$\beta/H_*$	Inverse PT duration	uniform $[5, 70]$
$T_*$	PT temperature	uniform $[0.01, 1.6]$
$\alpha_{PT}$	PT strength	uniform $[0.0, 1.0]$
$\nu_b$	Velocity of bubble wall	uniform $[0.9, 1.0]$
<b>Model-11: SIGW</b>		
$P_{R0}$	Amplitude of signal	log-uniform $[-4, -1.5]$
$n$	Slope of spectrum	uniform $[-2, 2]$

TABLE V. Bayes Factor of Model-2: dual scenario ( $w, r$ ) versus other Models

	SMBHBs	CS	DW	FOPT	SIGW
NG15	$94.6 \pm 34.9$	$461.6 \pm 127.2$	$318.8 \pm 73.3$	$61.4 \pm 11.6$	$65.2 \pm 12.4$
EPTA DR2	$3.9 \pm 1.6$	$3.1 \pm 1.2$	$30.5 \pm 8.0$	$3.2 \pm 0.7$	$6.0 \pm 1.4$
PPTA DR3	$22.3 \pm 9.1$	$16.4 \pm 7.1$	$19.9 \pm 8.9$	$6.4 \pm 2.4$	$12.1 \pm 4.2$
IPTA DR2	$3.8 \pm 2.0$	$7.6 \pm 3.4$	$7.3 \pm 3.7$	$2.8 \pm 1.1$	$13.9 \pm 6.2$

TABLE VI. Bayes Factor of Model-3: stable solutions ( $m, r$ ) versus other Models

	SMBHBs	CS	DW	FOPT	SIGW
NG15	$81.5 \pm 32.3$	$397.7 \pm 117.8$	$274.7 \pm 67.8$	$52.9 \pm 10.7$	$56.2 \pm 10.7$
EPTA DR2	$3.0 \pm 1.3$	$2.4 \pm 0.9$	$23.6 \pm 6.1$	$2.5 \pm 0.6$	$4.7 \pm 1.1$
PPTA DR3	$15.1 \pm 6.2$	$11.1 \pm 4.8$	$13.5 \pm 6.0$	$4.3 \pm 1.6$	$8.2 \pm 2.9$
IPTA DR2	$3.3 \pm 1.7$	$6.6 \pm 2.9$	$6.3 \pm 3.2$	$2.4 \pm 1.0$	$12.0 \pm 5.4$

TABLE VII. Bayes Factor of Model-4: dynamic solutions ( $m, r$ ) versus other Models

	SMBHBs	CS	DW	FOPT	SIGW
NG15	$49.4 \pm 17.3$	$240.7 \pm 63.2$	$166.3 \pm 36.4$	$32.0 \pm 6.8$	$34.0 \pm 6.5$
EPTA DR2	$2.3 \pm 0.9$	$1.8 \pm 0.7$	$17.7 \pm 4.4$	$1.9 \pm 0.4$	$3.5 \pm 0.8$
PPTA DR3	$12.3 \pm 5.0$	$9.0 \pm 3.9$	$11.0 \pm 4.9$	$3.5 \pm 1.3$	$6.7 \pm 2.3$
IPTA DR2	$2.2 \pm 1.1$	$4.4 \pm 1.9$	$4.2 \pm 2.2$	$1.6 \pm 0.7$	$8.0 \pm 3.6$

$$B_{ij}^{EPTA} = \begin{pmatrix} 1.0 & 0.8 \pm 0.4 & 7.8 \pm 3.1 & 0.8 \pm 0.3 & 1.5 \pm 0.6 \\ 1.3 \pm 0.6 & 1.0 & 9.9 \pm 3.6 & 1.1 \pm 0.4 & 2.0 \pm 0.6 \\ 0.1 \pm 0.1 & 0.1 \pm 0.04 & 1.0 & 0.1 \pm 0.02 & 0.2 \pm 0.1 \\ 1.2 \pm 0.5 & 1.0 \pm 0.3 & 9.4 \pm 1.8 & 1.0 & 1.9 \pm 0.4 \\ 0.6 \pm 0.2 & 0.5 \pm 0.2 & 5.0 \pm 1.3 & 0.5 \pm 0.1 & 1.0 \end{pmatrix} \quad (35)$$

$$B_{ij}^{PPTA} = \begin{pmatrix} 1.0 & 0.7 \pm 0.3 & 0.9 \pm 0.4 & 0.3 \pm 0.1 & 0.5 \pm 0.2 \\ 1.4 \pm 0.6 & 1.0 & 1.2 \pm 0.5 & 0.4 \pm 0.2 & 0.7 \pm 0.2 \\ 1.1 \pm 0.5 & 0.8 \pm 0.4 & 1.0 & 0.3 \pm 0.1 & 0.6 \pm 0.2 \\ 3.5 \pm 1.3 & 2.6 \pm 1.0 & 3.1 \pm 1.2 & 1.0 & 1.9 \pm 0.5 \\ 1.8 \pm 0.7 & 1.4 \pm 0.5 & 1.6 \pm 0.7 & 0.5 \pm 0.2 & 1.0 \end{pmatrix} \quad (36)$$

$$B_{ij}^{IPTA} = \begin{pmatrix} 1.0 & 2.0 \pm 1.1 & 1.9 \pm 1.1 & 0.8 \pm 0.4 & 3.7 \pm 1.7 \\ 0.5 \pm 0.3 & 1.0 & 1.0 \pm 0.5 & 0.4 \pm 0.1 & 1.8 \pm 0.7 \\ 0.5 \pm 0.3 & 1.0 \pm 0.5 & 1.0 & 0.4 \pm 0.2 & 1.9 \pm 0.5 \\ 1.3 \pm 0.6 & 2.7 \pm 1.0 & 2.6 \pm 1.2 & 1.0 & 4.9 \pm 1.5 \\ 0.3 \pm 0.01 & 0.6 \pm 0.2 & 0.5 \pm 0.5 & 0.2 \pm 0.1 & 1.0 \end{pmatrix} \quad (37)$$

**Nearly scale-invariant solutions ( $n_s - 1 = -0.04$ )**

For nearly scale-invariant solutions with  $n_s - 1 = -0.04$  from WMAP and Planck observations, their spectra (Eq.(21) and Eq.(22)) exhibit slight differences from the purely scale-invariant solutions (Eq.(19) and Eq.(20)) by a few percentages. The posterior distribution for these solutions is illustrated in Fig. 5, which closely resembles Fig. 2(c), as expected. This provides a cross-check for the results presented in the main text.



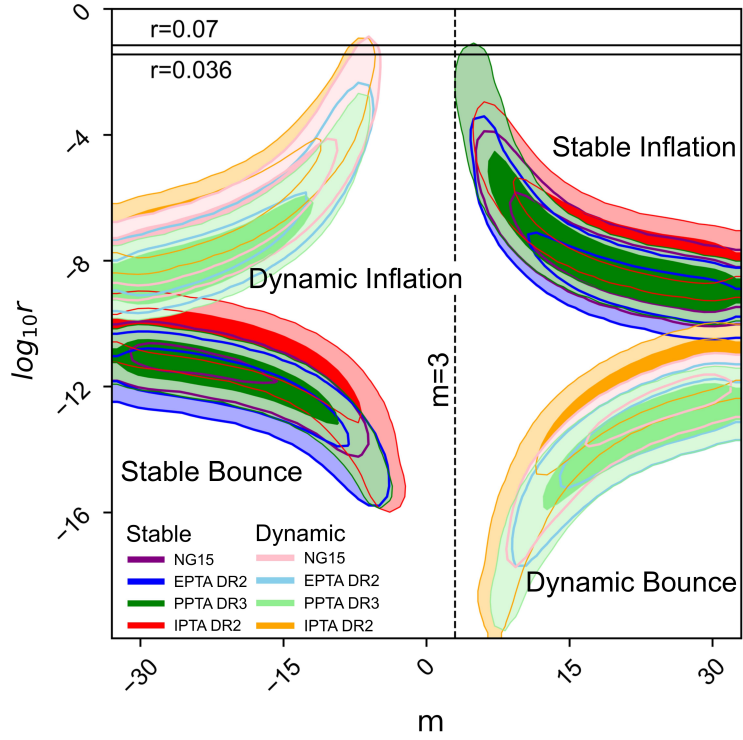


FIG. 5. The posterior distribution (at 68% and 95% confidence levels) in the parameter space  $(m, r)$  of the nearly scale-invariant solutions (Eq.(21) and Eq.(22)) of dual scenario of generalized inflation and bounce cosmologies.